A Geometrically Calibrated Pinhole Camera Model for Single Viewpoint Omnidirectional Imaging Systems

Abstract

This paper presents a perspective imaging model that is able to display undistorted images captured with uncalibrated cameras on a cylindrical virtual screen and to detect the correct location of the viewing point respectively. By using a calibration pattern and thus avoiding complicated mathematical models, the optical center can be detected by tracking the optical rays generated by pairs of 3D points that have the same projection on the image plane. The calibration pattern is also used in order to generate normalized virtual screens on which captured images are back projected, a process that eliminates the deformations. Experimental results for single viewpoint omnidirectional cameras demonstrate the effectiveness of our method.

1 Introduction

Several techniques have appeared in the last decade capable of recovering complete three dimensional information from multiple images. They employ either calibrated or uncalibrated cameras, with perspective projection serving as the dominant imaging model. In our assumption, in a perspective projection imaging model, straight lines in the scene are projected as straight lines in the image, while in a non perspective projection model, straight lines in the scene appear as curved in the image.

This paper is presenting a perspective imaging model that enables a distortion free display on a cylindrical virtual screen of the images captured with an uncalibrated, singleviewpoint, omnidirectional camera, supplemented by a precise detection of its optical center. Essentially, this imaging model can be regarded as a calibrated omnidirectional pinhole camera model.

An important feature of algorithms using uncalibrated cameras is that no knowledge of the internal or external parameters of the camera is required. However, no lens is perfect. In the presence of nonlinear lens distortion the pinhole camera model is no longer valid and the technique breaks down. On the other hand, mathematical models of lens distortion developed for calibrated cameras compensated the errors but could not completely eliminate them.

A solution to these problems would be a geometric camera calibration. For example, by measuring the line-of-sight vector at each pixel in the image, a lookup table could be generated and then, for any pixel in an image, simple indexing would yield the line-of-sight vector. A complete geometric camera calibration includes the projection problem (for a given point in space predict its location in the image) and the back-projection problem (for a given pixel in the image compute the line-of-sight vector through the pixel).

In their work, Gremban et al. [8] succeeded in offering a complete solution to the geometric camera calibration problem for the case of conventional cameras. Their method was based on a two-plane method of Martins et al. [9] but was extended to include a solution to the projection problem as well. Compared to their work, our technique for detecting the optical center (the projection problem) uses the same principle of two calibration objects in order to find pairs of

BMVC 2004 doi:10.5244/C.18.40

3D points that are projected on the same pixel of the camera's image plane. The rays of light generated by these pairs of corresponding points converge at the optical center of the imaging model. The originality of our technique is related to the way the calibration patterns are generated and to the method of estimating the accuracy of the results. Moreover, our model allows a visualization of the rays of light and of the optical center.

In order to offer a complete solution to the geometric calibration problem of the single viewpoint omnidirectional camera, we built cylindrical virtual screens that had the same shape as the calibration pattern. The images taken with an uncalibrated camera are then back-projected on these virtual screens based on a combination of linear and circular interpolation techniques. Because the virtual screens resemble the exact shape of the calibration patterns, this back-projection process can be seen as an image plane normalization.

Recently, the developments in image sensing applications have restricted the usefulness of the perspective model. In order to represent any imaging system, Grossberg [1] introduced a new imaging model that was based on determining the locus of viewpoints (i.e. the caustic) of an imaging system by using the Jacobian method. While their method determines the envelope of the reflected rays (i.e. the catacaustic Figure 1a), in our work we are estimating the point of intersection of the incident rays. Moreover, in their calibration technique of the rotationally symetric imaging systems, they neglected a practical aspect that is the deviation between the rotation axis and the location of the optical center (Figure 1b). This deviation will obstruct the correct convergence of the reflected rays toward the optical center of the camera. Our research introduces an original method to compensate this deviation.

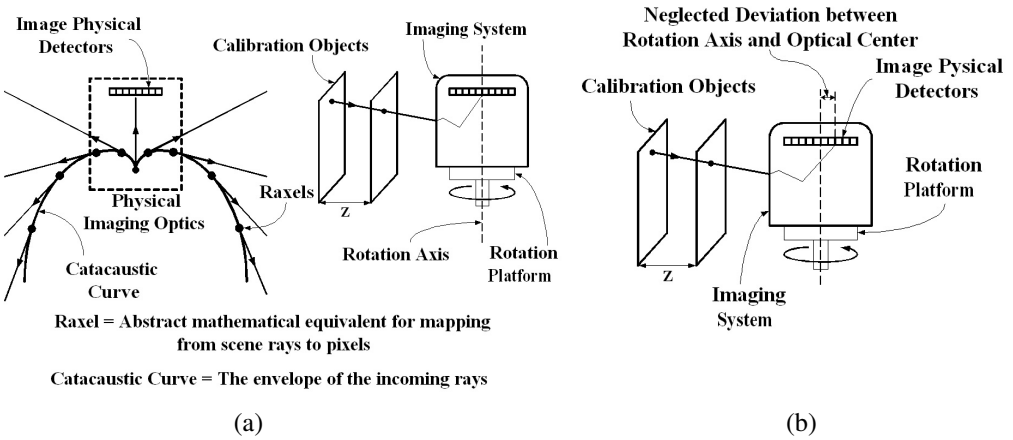

Figure 1: (a) Grossberg's imaging model and its calibration technique. (b) The neglected deviation.

A geometric method for estimating the intrinsic parameters of a catadioptric system consisting of a parabolic mirror and an orthographic lens have been investigated by Geyer and Daniilidis [2]. They introduced the geometry of catadioptric line projection and showed that the vanishing points lie on a conic section which encodes the entire calibration information. Aliaga [3] used an omnidirectional camera based on the design of Nayar [4] to develop a calibration model that relaxes the assumption of an ideal projection system and compensates for mild perspective projections in addition to radial distortion and mirror misalignment.

The projection of undistorted images on virtual screens was used by Yamazawa [5]. They used a grid pattern and by employing a bilinear interpolation process they projected the captured image onto rectilinear virtual screen. In this way they succeeded to eliminate the errors induced by lens artifacts. To perform the camera calibration they subsequently applied Tsai's method [6].

This paper is organized as follows. The basic principles of our approach are shown in Section 2 while in Section 3 we describe the 3D solution we used for estimating the point of convergence of rays of light. Finally, Sections 4 and 5 give our experimental results and conclusion.

2 Geometric Omnidirectional Camera Calibration

We used a catadioptric system consisting of a perspective camera looking into a hyperbolic mirror. In order to generate a distortion free representation of the captured image, we performed an image plane normalization. Because the omnidirectional camera had a 360 degrees field of view, we built a cylindrical shaped calibration object by placing an LED bar (consisting of 72 LEDs) at a certain distance from the omnidirectional camera and computed the locations of each LED for intermediate positions from 15 to 15 degrees (Figure 2).

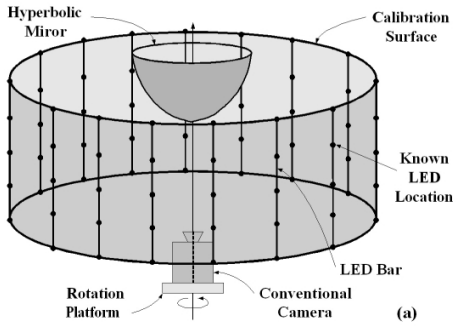

Figure 2: Cylindrical shaped calibration object.

The normalization process required building a virtual screen that necessarily had the same shape as the calibration object. We built our virtual screen as a scaled representation of the generated cylinder shaped calibration object. This was followed by a back-projection of the captured images onto the screen. The back-projection task was performed by employing local linear and circular interpolation that computed the corresponding image pixel for each point on the virtual screen (see Figure 3a). Figure 3b illustrates the interpolation method on the image plane.

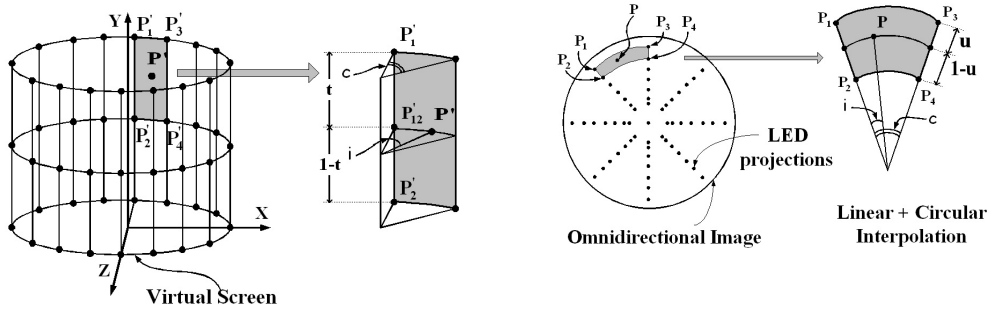

Figure 3: Back-projection performed by local interpolation: (a) on virtual screen; (b) on omnidirectional image.

In the case of catadioptric systems with hyperbolic mirrors (Figure 4), all the reflected rays $\mathbf{p}'$ intersect at the focal point of the mirror $\mathbf{F}'$ and the camera center of projection **C** coincides with the second focal point of the mirror, **F**. Because of the uniqueness of the projection center **C**, if two 3D points from the surrounding environment have the same representation on the image plane we can say that they lie on the same reflected ray that will also include the mirror's focal point. Our purpose is to find the optical center which is identical to the mirror's focal point.

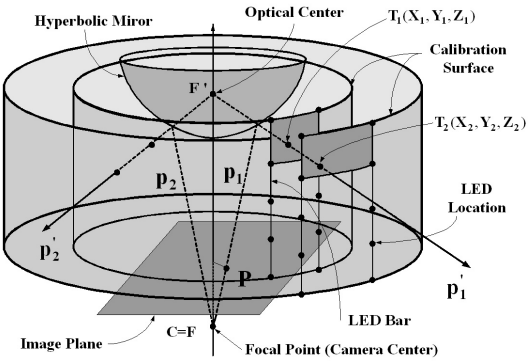

Figure 4: Optical center detection for Single Viewpoint Omnidirectional Camera

In order to detect the location of the optical center, it is necessary to track the converging optical rays. Accordingly, we generated two cylinder shaped calibration surfaces and computed the corresponding 3D points that are projected onto the same pixel on the image plane (Figure 4).

Beginning with the known coordinates of both the LEDs on the calibration pattern and their projections on the image plane, a correspondence can be established between each pixel in the image plane and 3D points on the calibration pattern. This is done by applying the same interpolating technique to both the calibration surface and image plane. For each intermediate distance, we built a lookup table that matched the pixels in the image plane with the corresponding 3D points located on the calibration surface. By performing a search on the resulting two tables, the pairs of 3D points that correspond to the same pixels could be easily identified.

3 Estimating the Optical Center

Two lines in 3D generally don't intersect at a point. They may be parallel (no intersection) or they may be coincident (infinite number of intersections) but most often only their projection onto a plane actually intersects. When they don't exactly intersect at a point they can be connected by a line segment, the shortest possible line segment is unique and often considered to be the equivalent of their intersection in 3D.

In order to find the point that is located at the shortest distance to all of the generated rays of light, we proceeded to the use the linear least-squares method which computes an approximate solution by minimizing the sum of all the distances from an arbitrary point to all the rays.

Considering Figure 5, the vector **OR** from an arbitrary point **O** to a line **d** in the direction of a vector **v** that includes point **P** can be expressed as follows:

$$\mathbf{OR} = \mathbf{PR} - \mathbf{PO}$$

$$\text{with } \mathbf{PR} = (\mathbf{PO} \cdot \mathbf{v})\,\mathbf{v} = \mathbf{v}^T\mathbf{PO}\,\mathbf{v}$$

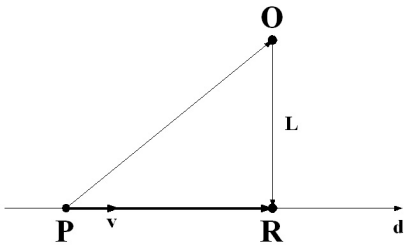

Figure 5: Distance from a Point to a Given Line

As a result:

$$\mathbf{OR} = \mathbf{v}^T\mathbf{PO}\,\mathbf{v} - \mathbf{PO} = \mathbf{v}^T(\mathbf{P}-\mathbf{O})\,\mathbf{v} - (\mathbf{P}-\mathbf{O}) =$$
$$= \mathbf{v}^T\mathbf{P}\,\mathbf{v} - \mathbf{v}^T\mathbf{O}\,\mathbf{v} - \mathbf{P} + \mathbf{O}$$

Having given 3-D coordinates of

$$\mathbf{P} = \begin{pmatrix} x_0 \\ y_0 \\ z_0 \end{pmatrix}, \mathbf{O} = \begin{pmatrix} x \\ y \\ z \end{pmatrix} \text{ and } \mathbf{v} = \begin{pmatrix} v_x \\ v_y \\ v_z \end{pmatrix},$$

distance

$$\mathbf{L} = \| \mathbf{OR} \|$$

can than be expressed as:

$$\mathbf{L} = \mathbf{AX} - \mathbf{B}$$

with

$$\mathbf{A} = \begin{pmatrix} v_xv_x - 1 & v_xv_y & v_xv_y \\ v_xv_y & v_yv_y - 1 & v_yv_z \\ v_xv_z & v_yv_z & v_zv_z - 1 \end{pmatrix}, \ \mathbf{B} = \begin{pmatrix} (v_xv_x - 1)x_0 + v_xv_yy_0 + v_xv_zz_0 \\ v_xv_yx_0 + (v_yv_y - 1)y_0 + v_yv_zz_0 \\ v_xv_zx_0 + v_yv_zy_0 + (v_zv_z - 1)z_0 \end{pmatrix}$$

$$\text{and } \mathbf{X} = \begin{pmatrix} x \\ y \\ z \end{pmatrix}.$$

The condition that point **O** will have to satisfy in order to coincide with the defacto converging point of a number of n rays of light will be:

$$\mathbf{L}_i = 0 \text{ for } i = 1..n$$

were $\mathbf{L}_i$ is the distance from point **O** to ray *i*.

This is the equivalent of a linear system of equations

$$\mathbf{A}_i\mathbf{X} = \mathbf{B}_i \text{ for } i = 1..n$$

whose solution is

$$\mathbf{X} = \frac{\mathbf{A}^T\mathbf{B}}{\mathbf{A}^T\mathbf{A}} \text{ with } \mathbf{A} = \begin{pmatrix} \mathbf{A}_1 \\ \mathbf{A}_2 \\ \vdots \\ \mathbf{A}_n \end{pmatrix}, \mathbf{B} = \begin{pmatrix} \mathbf{B}_1 \\ \mathbf{B}_2 \\ \vdots \\ \mathbf{B}_n \end{pmatrix}$$

and $\mathbf{A}_i, \mathbf{B}_i$ being the corresponding **A** and **B** for line $i = 1..n$.

4 Experimental results

The calibration setup consisted of: (1) a calibration pattern (an LED bar, the lighting of which was controlled by software), (2) an analog color camera with a resolution of 640 x 480 pixels, (3) a catadioptric attachment (paraboloid mirror), (4) a sliding rail, (5) a Pan-Tilt Unit (controlled by software). For both experiments we used a 2GHz PC with 2GB memory and a video capture board.

In the experiments, the sliding rail was oriented perpendicular towards the rotation axis of the omnidirectional camera as marked by the manufacturer of the catadioptric attachment. The origin of the world coordinate system was placed inside of the calibration patterns, with its equivalent virtual representation built with the XOZ plane parallel to the ground (see Figure 3a). The measurements were performed by placing the calibration pattern at respectively 13cm and 33cm away from the camera.

The generated rays of light will include the optical center if the vertical axes of the LED bar for a certain rotation angle are coplanar with the rotation axis of the camera (Figure 6 a). If this condition is not achieved and if a deviation angle is inserted, the 3D coordinates of the LEDs will be wrongly estimated and the location of the optical center will be missed (Figure 6 b), as has not been addressed previously.

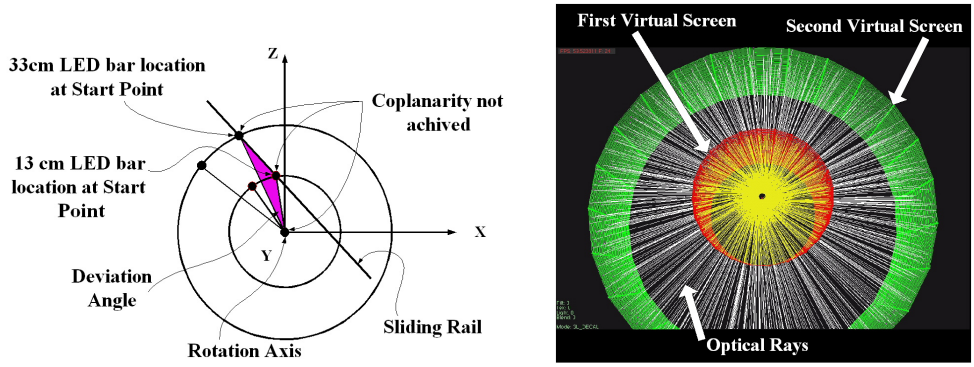

(a) (b)

Figure 6: (a) Top view of the wrong alignment condition: Coplanarity is required in order to have convergent rays of light. (b) Top view of the virtual screens: Erroneous placement of the calibration pattern generates a locus of the optical center on the circumference of a circle, rather than at the true center.

In order to detect the deviation angle we applied the following method. First, we determined the parameters of the lines generated by the projections of LEDs on the image plane for two different camera-to-LED distances(Figure 7 a). We used the least-squares minimization method to approximate the best fitting lines. Further, we computed their intersecting points and the results obtained confirmed that they were indeed identical.

This outcome gave us the common element that was needed in order to compare the two sets of lines. The deviation between the corresponding lines to different distances represents the actual deviation inserted by erroneous placement of the LED bar. Once the deviation angle was identified, we constructed the calibration surfaces accordingly, the final result being presented in Figure 7 b.

The new results of the calibration process placed the optical center inside of the virtual screen with a remaining slight deviation from the rotation axis. In order to measure the error of the optical center estimation we computed the deviation of the optical center from the baseline generated

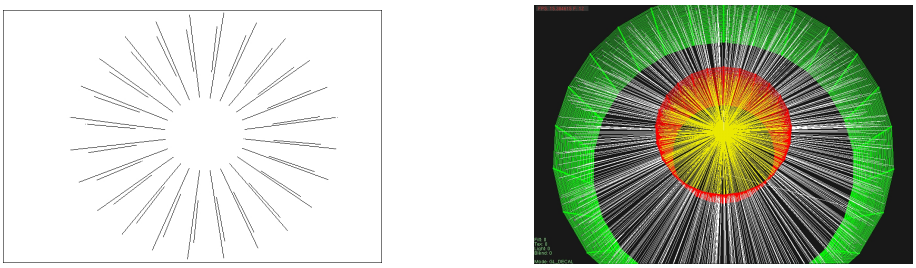

(a) (b)

Figure 7: (a) Lines through the sets of pixels representing the projections of LEDs for two consecutive distances. (b) After proper correction, the locus of the optical center will be a point.

by recording two images at different locations with the camera placed at the same height from the ground.

Using the fact that for the single viewpoint omnidirectional camera, we had represented the image plane via the cylindrical virtual screen, the intersection of the baseline with each corresponding virtual screen will generate two epipoles. Therefore, the direction of the baseline will coincide with the line generated by the epipoles on each virtual screen and our initial task will be reduced to computing the angular deviation of the estimated optical center with regard to the line generated by the epipoles that belong to the same virtual screen (Figure 8 a).

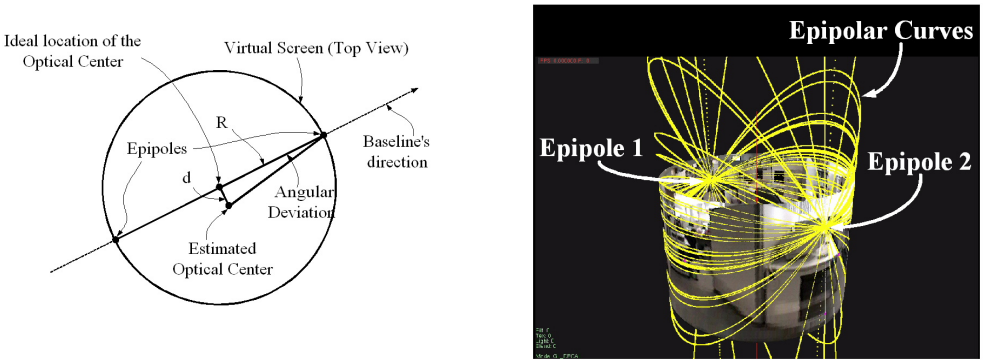

(a) (b)

Figure 8: (a) Computing the deviation from the baseline of the estimated optical center. (b) Optical Center Estimation.

We computed the coordinates of the two epipoles as the intersection points of the epipolar curves generated by using a set of 50 corresponding feature points placed uniformly around the surface of the virtual screen. Our method used Kanatani's [7] algorithm to compute the essential matrix which was then employed in the epipolar constraint equation to draw the epipolar curves. These and their epipoles are presented in Figure 8 b.

In order to check the correctness of the epipolar curves we had to verify if a given set of feature points in one image rests on the epipolar curves generated by the corresponding set of feature points from the other image. Our approach was to measure the angular deviation between a feature point and its corresponding nearest point located on the epipolar curve, with regard to the optical center (see Figure 9 a). For all 50 pairs we found a mean angular deviation of 0.297 degrees for the feature points.

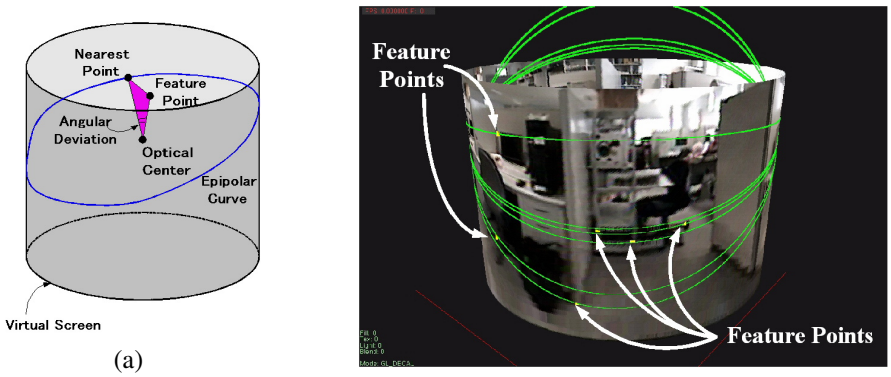

(a) (b)

Figure 9: Checking the correctness of the epipolar curves: (a) angular deviation; (b) six feature points and their corresponding epipolar curves.

Though 50 pairs were chosen to ensure coverage of the entire viewing field, Figure 8 b can be considered rather visually complex. Figure 9 b displays a much clearer picture of six of the feature points (white dots in the image) and the epipolar curves generated by corresponding feature points in the other image.

Based on our calculations (knowing the radius of the cylinder and computing the distance from the estimated optical center to the line generated by the epipoles) we obtained an angular deviation of 0.316 degrees for the estimated optical center. By combining back-projected images with the converging rays we get the final representations of the virtual screens and the optical center (Figure 10). As can be noticed, the objects in the normalized image are keeping their proportions.

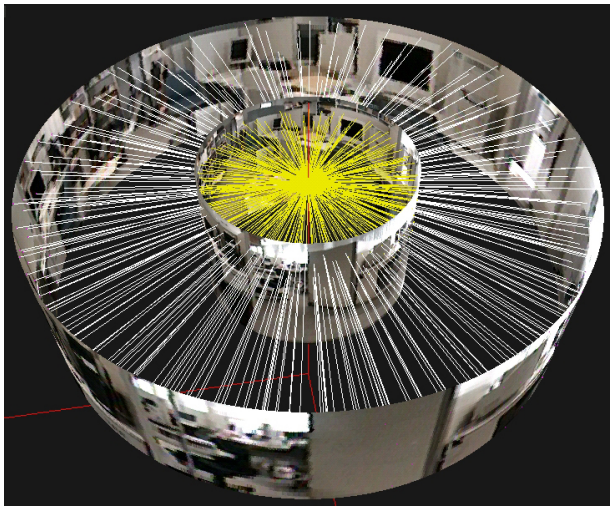

Figure 10: Converging rays for single viewpoint omnidirectional camera.

5 Summary and Conclusions

The main contribution of this paper was the presentation of a pinhole camera model that can be used to represent an omnidirectional single viewpoint imaging system. This model uses a calibration object in order to build a virtual screen on which undistorted images are projected. Moreover, it can detect and visualize the optical center by performing optical ray tracking. In the experiments, our results for omni-directional cameras demonstrated the effectiveness of this method. In the future we plan to extend our work into the simultaneous 3D reconstruction and localization tasks that are suitable for intelligent mobile robots.

References

[1] M.D. Grossberg, Shree K. Nayar. *A General Imaging Model and a Method for Finding its Parameters*. *Proceedings of ICCV*. 2001.

[2] C.Geyer and K.Daniilidis. *Catadioptric camera calibration*. in *Proceedings of the Seventh International Conference on Computer Vision*. September 1999, pp. 398–404.

[3] Daniel G. Aliaga. *Accurate catadioptric calibration for real-time pose estimation in room-size environments*. in *Proceedings of ICCV*. 2001, pp. 127–134.

[4] S.K. Nayar. *Catadioptric omnidirectional camera*. in *CVPR*. 1997, pp. 482–488.

[5] Y. Yagi K. Yamazawa and M. Yachida, *Omnidirectional imaging with hyperboloidal projection*. in *Proc. of the Int'l Conf. on Robots and Systems*. 1993.

[6] R.Y. Tsai. *A versatile camera calibration technique for high-accuracy 3d machine vision metrology using off-the-shelf tv cameras and lenses*. *IEEE J. of Robotics and Automation*. vol. RA-3(4), pp. 323–344, Aug. 1987.

[7] Kenichi Kanatani, "Optimal Fundamental Matrix Computation: Algorithm and Reliability Analysis," *6th Symposium on Sensing via Image Information (SII 2000)*, June 2000, Yokohama, Japan.

[8] Keith D. Gremban, Charles E. Torpe and Takeo Kanade "Geometric Camera Calibration using Systems of Linear Equations," *Proc. IEEE Int. Conf. on Robotics and Automation*, 2, 562/567, 1988.

[9] H. A. Martins, J. R. Birk and R. B. Kelly "Camera Models Based on Data from Two Calibration Planes," *Computer Graphics and Image Processing*, 17, 173/180, 1981.